

Scalable Uncertainty Quantification for Black-Box Density-Based Clustering

Nicola Bariletto

The University of Texas at Austin

Stephen G. Walker

The University of Texas at Austin

Abstract

We introduce a novel framework for uncertainty quantification in clustering. By combining the martingale posterior paradigm with density-based clustering, uncertainty in the estimated density is naturally propagated to the clustering structure. The approach scales effectively to high-dimensional and irregularly shaped data by leveraging modern neural density estimators and GPU-friendly parallel computation. We establish frequentist consistency guarantees and validate the methodology on synthetic and real data.

1 INTRODUCTION

This article introduces a novel approach for posterior uncertainty quantification in clustering applications. We build on recent advances in the Bayesian predictive approach (Fortini and Petrone, 2023, 2025), specifically martingale posterior distributions (Fong et al., 2023), which naturally provide full uncertainty quantification for the data-generating density. In line with the philosophy of density-based clustering, we cast cluster assignment purely as a function of the underlying density and its level sets Chacón (2015); Ester et al. (1996); Ankerst et al. (1999); Chazal et al. (2013). This formulation allows uncertainty in the density estimate to be propagated directly to the clustering structure, as supported by our theoretical study of the frequentist properties of the procedure.

Crucially for practical purposes, the Bayesian predictive framework—specifically the score-based version we adopt here—enables the use of modern flexible density estimators; for instance, in our numerical experiments, we employ normalizing flow architectures (Rezende and Mohamed, 2015; Papamakarios et al., 2021, 2017). Moreover, the resampling procedure can be efficiently parallelized on modern hardware such as GPUs. For these reasons, as we verify in our experiments, the proposed approach effectively captures

clustering uncertainty at a fraction of the computational cost of traditional MCMC methods, which typically struggle to scale with model flexibility and data dimensionality.

2 METHODOLOGY

Our contribution is grounded in two main methodological literatures: martingale posterior distributions (MPDs) and density-based clustering (DBC). We briefly introduce these two components below.

2.1 Score-Based Martingale Posteriors

Assume we observe a sample $X_{1:n} := (X_1, \dots, X_n)$ taking values in the sample space $\mathcal{X} \subseteq \mathbb{R}^p$ and generated i.i.d. from an unknown density f_* with respect to the Lebesgue measure λ on \mathcal{X} . At a basic level, the MPD framework treats uncertainty as arising from the missing tail of the observed data sequence (Fong et al., 2023). Uncertainty is therefore accounted for by imputing the tail recursively: first draw $Y_1 \sim \pi_{n,0}(\cdot | X_{1:n})$ to impute X_{n+1} , then draw $Y_2 \sim \pi_{n,1}(\cdot | X_{1:n}, Y_1)$ to impute X_{n+2} , and so on. The key ingredient of this procedure, referred to as *predictive resampling*, is a sequence $(\pi_{n,k})_{k \geq 0}$ of predictive distributions (PDs) that drive the recursive imputation. Once the entire sequence has been resampled, any identifiable parameter can be obtained as a deterministic function of it. The randomness induced by resampling therefore translates into randomness at the level of the parameter, which is said to be drawn from the *martingale posterior distribution*.

An appealing predictive resampling strategy in the context of density estimation, particularly in light of modern deep learning architectures, is the following. Suppose that, based on the observed data $X_{1:n}$, we have trained a differentiable density estimator $\{f_\theta(x) : \theta \in \Theta\}$ with closed parameter space $\Theta \subseteq \mathbb{R}^d$. Let $s(x; \theta) := \nabla_\theta \log f_\theta(x)$ denote the associated *score*, and let $\theta_{n,0}$ be the trained parameter. Fix a learning rate schedule $\eta_{n,k} := \eta_0 / (n + k - 1)$ for some $\eta_0 > 0$, and

consider the scheme

$$Y_k \mid Y_{1:k-1} \sim f_{\theta_{n,k-1}},$$

$$\theta_{n,k} = \theta_{n,k-1} + \eta_{n,k} s(Y_k; \theta_{n,k-1}),$$

for all $k \geq 1$, with $Y_1 \sim f_{\theta_{n,0}}$ when $k = 1$ (Cui and Walker, 2025; Fortini and Petrone, 2025). Intuitively, the sequence $(\theta_{n,k})_{k \in \mathbb{N}}$ forms a martingale because of the score identity $\mathbb{E}_{Y \sim f_\theta} [s(Y; \theta)] = 0$, which holds under mild regularity conditions on the density estimator. The limiting distribution of this martingale coincides with the MPD of interest. In practice, the latter is approximated by stopping the predictive resampling procedure after a large but finite number of steps $k = N$.

For the MPD to be well defined, the predictive resampling procedure must converge, or equivalently the random limit $\lim_{N \rightarrow \infty} \theta_{n,N}$ must exist. To formalize this, introduce an algorithmic probability space $(\Omega, \mathcal{F}, \mathbb{P})$ on which the predictive resampling procedure is defined and governed by the probability measure \mathbb{P} . In this setting, let $(\mathcal{F}_k)_{k \in \mathbb{N}}$ denote the filtration generated by $(Y_k)_{k \in \mathbb{N}}$, with respect to which $(\theta_{n,k})_{k \in \mathbb{N}}$ is adapted.

Theorem 1. *Assume that*

- for all $\theta \in \Theta$, $\mathbb{E}_{Y \sim f_\theta} [s(Y; \theta)] = \nabla_\theta \mathbb{E}[\log f_\theta(Y)]$,
- $\sup_{\theta \in \Theta} \mathbb{E}_{Y \sim f_\theta} [\|s(Y; \theta)\|^2] \leq M$ for some $M < \infty$.

Then $\theta_{n,\infty} := \lim_{N \rightarrow \infty} \theta_{n,N}$ is a well-defined random variable on $(\Omega, \mathcal{F}, \mathbb{P})$.

Denote by $\Pi_n := \mathbb{P} \circ \theta_{n,\infty}^{-1}$ the induced distribution on Θ . This is the MPD, which encodes uncertainty over the parameter.¹

2.2 Density-Based Clustering

Clustering is a fundamental unsupervised learning task aimed at identifying distinct homogeneous subpopulations within a reference population. The statistics and machine learning communities have framed this problem in several ways. In statistics, a particularly popular approach is *model-based clustering* (McLachlan and Peel, 2000; Fraley and Raftery, 2002), which defines clusters as subgroups of observations generated by the same kernel component of a density mixture model.

A different approach, adopted here and known as *density-based clustering*, defines clusters purely as a functional of a given density (Chacón, 2015). There are several DBC methods, but perhaps the most basic

¹In the remainder of the paper, we silently assume that the conditions of Theorem 1 hold.

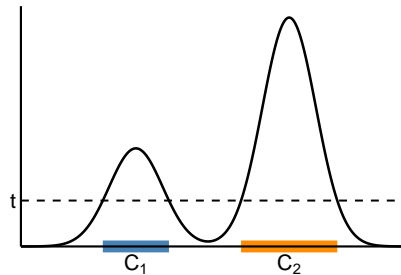


Figure 1: Illustration of DBC. The plotted density has two clusters, labeled C_1 and C_2 , corresponding to the two connected components of the upper-level set at level t .

one is as follows.² Given a density $f : \mathcal{X} \rightarrow [0, \infty)$ and $t \in (0, \infty)$, let $\mathcal{L}_t(f) := \{x \in \mathcal{X} : f(x) \geq t\}$ denote the *upper-level set* of f at level t . Define $\mathcal{C}_t(f)$ as the set of path-connected components (that is, maximal path-connected subsets) of $\mathcal{L}_t(f)$.³ The elements of $\mathcal{C}_t(f)$ are called the clusters of f at level t , and $k_f(t) := |\mathcal{C}_t(f)|$ denotes the number of such clusters. Figure 1 illustrates this construction. In practice, given data, one typically first estimates the unknown generating density f_* and then performs clustering based on the resulting estimate, assigning data points to the obtained clusters.⁴

Compared to model-based clustering, DBC has several appealing features. It is robust to the shape of the clusters, whereas good clustering performance with mixtures relies on a well-specified kernel choice. DBC is also adaptable to very general sample spaces (Chazal et al., 2013), and it does not rely on a specific density model such as mixtures; this allows one to exploit density estimation paradigms that adapt well to high-dimensional settings. Most importantly for our purposes, DBC defines clustering purely as a function of the underlying density. As a consequence, clustering becomes an *identifiable parameter* whenever the density is identifiable.⁵ This property makes DBC

²This roughly corresponds to the seminal DBSCAN algorithm (Ester et al., 1996).

³A subset A of \mathcal{X} is said to be path-connected if for any two points $x, y \in A$ there exists a continuous path connecting them that lies entirely in A . See the Supplementary Materials for further details.

⁴Some points may fall outside the upper-level sets and thus not belong to any cluster. These can either be classified as noise or assigned to the nearest cluster. Throughout our experiments, we adopt the second strategy, as it is often insightful to provide a complete clustering picture of the whole dataset at hand.

⁵This contrasts with model-based clustering, where cluster membership is not identifiable from a density alone and exists only at the latent level.

particularly well suited to the predictive resampling framework described in the previous section, since uncertainty in the density f directly induces uncertainty in $\mathcal{C}_t(f)$.

2.3 Combining MPDs and DBC

Our key contribution is to provide MPD-based uncertainty quantification for DBC procedures. The approach is straightforward: suppose we have a density estimate $f_{\theta_{n,0}}$ trained on the available data. We then perform predictive resampling T times independently for N steps (with N large), obtaining T MPD samples of the density, $f_{\theta_{n,N}^1}, \dots, f_{\theta_{n,N}^T}$. Finally, for each resampled density, we perform DBC, for instance with the upper-level set method described above, enabling uncertainty quantification at the level of the clustering. The procedure is particularly appealing because the T resamples are fully independent, gradient-based, and can be executed in parallel, making the pipeline highly compatible with modern hardware such as GPUs.

3 FREQUENTIST GUARANTEES

We now study the asymptotic properties of our methodology when DBC is performed through the upper-level set procedure described in Subsection 2.2. We adopt the frequentist assumption that the data are i.i.d. from an unknown distribution F_* with density f_* .⁶ Our strategy is to translate convergence of the estimator $f_{\theta_{n,0}}$ into contraction of the MPD for the density, and then into consistency of the induced clustering.

3.1 Density Consistency

We first establish contraction of the MPD at the level of the density. Let d be a metric between densities (e.g., Hellinger or \mathcal{L}^p). For a positive vanishing sequence $(\varepsilon_n)_{n \in \mathbb{N}}$, we say that $f_{\theta_{n,0}}$ is (d, ε_n) -consistent at f_* if

$$\lim_{n \rightarrow \infty} F_*^n(d(f_{\theta_{n,0}}, f_*) > \varepsilon_n) = 0.$$

The following result links the rate ε_n to contraction of the MPD.⁷

Theorem 2. *Assume there exist $L > 0$ and $\gamma \in (0, 1]$ such that $d(f_\theta, f_{\theta'}) \leq L \|\theta - \theta'\|^\gamma$ for all $\theta, \theta' \in \Theta$. If $f_{\theta_{n,0}}$ is (d, ε_n) -consistent at f_* , then*

$$\lim_{n \rightarrow \infty} \Pi_n(\theta : d(f_\theta, f_*) > \tilde{\varepsilon}_n) = 0 \quad \text{in } F_*^n\text{-prob.} \quad (1)$$

for any decreasing sequence $\tilde{\varepsilon}_n \gtrsim \varepsilon_n$ satisfying $\lim_{n \rightarrow \infty} n \tilde{\varepsilon}_n^{2/\gamma} = \infty$.

⁶We denote by F_*^n the n -fold product measure induced by F_* .

⁷See Fong and Yiu (2024, 2025) for related results.

3.2 Clustering Consistency

We now turn to clustering consistency.⁸ We assume that the true density f_* and all densities in the model class belong to a regular class of functions whose level sets have a finite number of path-connected components, and denote by $\mathcal{C}(f_*) = \{C_1(f_*), \dots, C_{k_{f_*}}(f_*)\}$ the clusters of the true density.

Let $A \Delta B := (A \setminus B) \cup (B \setminus A)$ denote the symmetric difference between sets A and B , and let S_k be the set of permutations of $\{1, \dots, k\}$. For densities f and f' with $k_f = k_{f'}$, we measure the discrepancy between the induced clusterings as follows (Rinaldo and Wasserman, 2010; Wang et al., 2019):

$$\mathcal{D}(\mathcal{C}(f), \mathcal{C}(f')) := \inf_{\sigma \in S_{k_f}} \sum_{j=1}^{k_f} \lambda(C_j(f) \Delta C_{\sigma(j)}(f')).$$

Theorem 3. *Assume f_* satisfies conditions (a), (b), and (c) in the Supplementary Materials A.3. If the assumptions of Theorem 2 hold and $\tilde{\varepsilon}_n$ is a contraction rate as in (1) for $d(f, f') = \|f - f'\|_{\mathcal{L}^\infty}$, then*

$$\lim_{n \rightarrow \infty} \Pi_n(f : k_f \neq k_{f_*}) = 0 \quad \text{in } F_*^n\text{-prob.} \quad (2)$$

and

$$\begin{aligned} \lim_{n \rightarrow \infty} \Pi_n \left(f : k_f = k_{f_*}, \mathcal{D}(\mathcal{C}(f), \mathcal{C}(f_*)) > k_{f_*} C_0 \tilde{\varepsilon}_n \right) \\ = 0 \quad \text{in } F_*^n\text{-prob.} \end{aligned} \quad (3)$$

4 NUMERICAL EXPERIMENTS

We demonstrate our methodology on two datasets. In both cases, a Masked Autoregressive Flow (MAF; Papamakarios et al., 2017) is trained to estimate the underlying density, followed by predictive resampling to quantify clustering uncertainty. The combined training, resampling, and clustering steps take under five minutes per dataset when parallelized on a single NVIDIA RTX A4000 GPU. This provides a scalable alternative to traditional MCMC-based Bayesian approaches, which struggle or become infeasible with irregular cluster shapes and high-dimensional data.

4.1 Noisy Concentric Circles

We first consider a two-dimensional dataset of $n = 5,000$ observations sampled from two noisy concentric circles, a classical example where model-based clustering fails due to the irregular shape of the clusters. After training the density estimator, we generate 1,000

⁸From this point on we fix the level $t = c$ and omit c from the notation. Without loss of generality, we also treat Π_n as a distribution over densities rather than parameters.

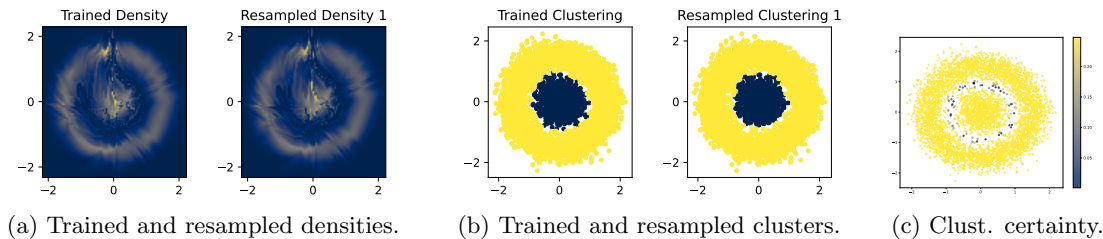


Figure 2: Noisy concentric circles experiment.

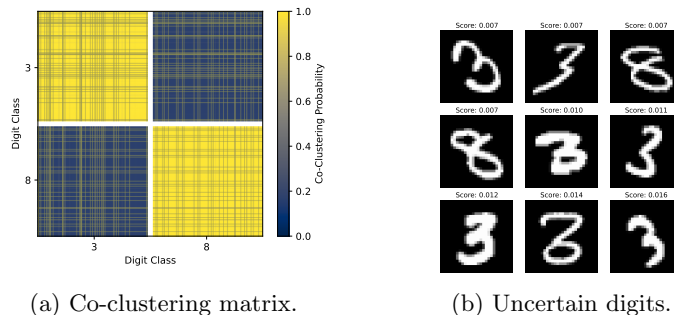


Figure 3: MNIST digits experiment.

independent predictive resamples of the density. Figure 2a shows that the resampled densities appear as perturbations of the trained estimate.

For each resampled density we perform upper-level set clustering, yielding samples from the martingale posterior over clusterings (Figure 2b). From these samples we compute the co-clustering matrix \mathcal{M} , where $\mathcal{M}(i, j)$ records the proportion of resamples in which points i and j are assigned to the same cluster. Figure 2c displays a simple derived measure of point-wise co-clustering certainty, $\mathcal{S}(i) := n^{-1} \sum_{j=1}^n (\mathcal{M}(i, j) - 0.5)^2$. Points near the boundary between the two circles exhibit the highest posterior uncertainty, indicating that the method effectively captures ambiguity in the clustering structure.

4.2 MNIST Digits

We next consider a subset of 5,000 images from the MNIST dataset (LeCun et al., 1998) containing a balanced number of digits 3 and 8, two classes that are visually similar. The images are first embedded into a 24-dimensional latent space using a convolutional autoencoder, after which the MAF density estimator is fitted to the encoded data. Clustering is then performed using the ToMATo algorithm (Chazal et al., 2013), a popular DBC algorithm that treats clusters as persistent level set connected components.

Figure 3a shows the posterior co-clustering matrix obtained from predictive resampling. While some un-

certainty is present, the posterior clustering structure largely agrees with the true labels. Figure 3b further shows that the digits with the highest posterior uncertainty (lowest $\mathcal{S}(\cdot)$) tend to have ambiguous shapes, such as 3’s with closed or nearly closed loops. Moreover, using the recently introduced methodology of Bariletto et al. (2025), we find that the true labeling belongs to a credible set with guaranteed 90% coverage under the MPD, highlighting the value of uncertainty quantification for robust clustering analysis of high-dimensional data with ambiguous separation structure.

5 CONCLUSION

We introduced a framework for uncertainty quantification in clustering by combining martingale posterior distributions with density-based clustering, propagating uncertainty from the estimated density directly to the clustering structure. Our results confirm the promise of the martingale posterior framework as a principled and scalable approach to uncertainty quantification for modern machine learning pipelines.

References

- Ankerst, M., Breunig, M. M., Kriegel, H.-P., and Sander, J. (1999). OPTICS: Ordering points to identify the clustering structure. *ACM SIGMOD Record*, 28(2):49–60.
- Bariletto, N., Ho, N., and Rinaldo, A. (2025). Con-

- formalized Bayesian Inference, with Applications to Random Partition Models. *arXiv preprint arXiv:2511.05746*.
- Chacón, J. E. (2015). A population background for nonparametric density-based clustering. *Statistical Science*, 30(4):518–532.
- Chazal, F., Guibas, L. J., Oudot, S. Y., and Skraba, P. (2013). Persistence-based clustering in Riemannian manifolds. *Journal of the ACM (JACM)*, 60(6):1–38.
- Cui, F. and Walker, S. G. (2025). Martingale posteriors from score functions. *arXiv preprint arXiv:2501.01890*.
- Dirmeier, S. (2024). Surjectors: surjection layers for density estimation with normalizing flows. *Journal of Open Source Software*, 9(94):6188.
- Ester, M., Kriegel, H.-P., Sander, J., and Xu, X. (1996). A density-based algorithm for discovering clusters in large spatial databases with noise. In *Proceedings of the Second International Conference on Knowledge Discovery and Data Mining (KDD-96)*, pages 226–231.
- Fong, E., Holmes, C., and Walker, S. G. (2023). Martingale posterior distributions. *Journal of the Royal Statistical Society Series B: Statistical Methodology*, 85(5):1357–1391.
- Fong, E. and Yiu, A. (2024). Asymptotics for parametric martingale posteriors. *arXiv preprint arXiv:2410.17692*.
- Fong, E. and Yiu, A. (2025). Bayesian quantile estimation and regression with martingale posteriors. *Journal of the Royal Statistical Society Series B: Statistical Methodology*.
- Fortini, S. and Petrone, S. (2023). Prediction-based uncertainty quantification for exchangeable sequences. *Philosophical Transactions of the Royal Society A: Mathematical, Physical and Engineering Sciences*, 381(2247).
- Fortini, S. and Petrone, S. (2025). Exchangeability, prediction and predictive modeling in Bayesian statistics. *Statistical Science*, 40(1):40–67.
- Fraley, C. and Raftery, A. E. (2002). Model-based clustering, discriminant analysis, and density estimation. *Journal of the American Statistical Association*, 97(458):611–631.
- Germain, M., Gregor, K., Murray, I., and Larochelle, H. (2015). MADE: Masked autoencoder for distribution estimation. In *International Conference on Machine Learning*.
- Kingma, D. P. and Ba, J. (2015). Adam: A method for stochastic optimization. In *International Conference on Learning Representations*.
- LeCun, Y., Bottou, L., Bengio, Y., and Haffner, P. (1998). Gradient-based learning applied to document recognition. *Proceedings of the IEEE*, 86(11):2278–2324.
- Loshchilov, I. and Hutter, F. (2019). Decoupled weight decay regularization. In *International Conference on Learning Representations*.
- McLachlan, G. J. and Peel, D. (2000). *Finite Mixture Models*. John Wiley & Sons.
- Papamakarios, G., Nalisnick, E., Rezende, D. J., Mohamed, S., and Lakshminarayanan, B. (2021). Normalizing flows for probabilistic modeling and inference. *Journal of Machine Learning Research*, 22(57):1–64.
- Papamakarios, G., Pavlakou, T., and Murray, I. (2017). Masked autoregressive flow for density estimation. In *Advances in neural information processing systems*.
- Rezende, D. J. and Mohamed, S. (2015). Variational inference with normalizing flows. In *International Conference on Machine Learning*.
- Rinaldo, A. and Wasserman, L. (2010). Generalized density clustering. *The Annals of Statistics*, 38(5):2678–2722.
- Wang, D., Lu, X., and Rinaldo, A. (2019). DBSCAN: Optimal rates for density-based cluster estimation. *Journal of Machine Learning Research*, 20(170):1–50.

Scalable Uncertainty Quantification for Black-Box Density-Based Clustering: Supplementary Materials

A MATHEMATICAL PROOFS

In this appendix, we report the proofs of each theoretical result presented in the main body of the article.

A.1 Proof of Theorem 1

Because $Y_k \mid \mathcal{F}_{k-1} \sim f_{\theta_{n,k-1}}$ and by assumption we can switch gradients and expectations, we have $\mathbb{E}[s(Y_k; \theta_{n,k-1}) \mid \mathcal{F}_{k-1}] = 0$. Hence $(\theta_{n,k})_{k \geq 0}$ is a martingale. By orthogonality of martingale increments and the uniform bound on the variance of the score,

$$\mathbb{E}[\|\theta_{n,N} - \theta_{n,0}\|^2] = \sum_{k=1}^N \eta_{n,k}^2 \mathbb{E}[\|s(Y_k; \theta_{n,k-1})\|^2] \leq V \sum_{k=1}^{\infty} \frac{\eta_0^2}{(n+k-1)^2} \leq \frac{V\eta_0^2}{n-1}. \quad (4)$$

Because

$$\mathbb{E}[\|\theta_{n,N}\|^2] \leq \mathbb{E}[\|\theta_{n,N} - \theta_{n,0}\|^2] + \|\theta_{n,0}\|^2 + 2\|\theta_{n,0}\|(\mathbb{E}[\|\theta_{n,N} - \theta_{n,0}\|^2])^{1/2} \leq \left(\frac{\sqrt{V}\eta_0}{\sqrt{n-1}} + \|\theta_{n,0}\| \right)^2$$

uniformly over N , $(\theta_{n,k})_{k \in \mathbb{N}}$ is an L^2 -bounded martingale, so Doob's L^2 martingale convergence theorem ensures existence of the \mathbb{P} -a.s. and L^2 limit $\theta_{n,\infty} := \lim_{n \rightarrow \infty} \theta_{n,N}$.

A.2 Proof of Theorem 2

We first fix an infinite data sequence $X_{1:\infty}$ and work on the algorithm probability space $(\Omega, \mathcal{F}, \mathbb{P})$, therefore treating $\theta_{n,0}$ as deterministic for now.

Applying the continuity of norms and Fatou's lemma to Equation (4), we get

$$\mathbb{E}[\|\theta_{n,\infty} - \theta_{n,0}\|^2] = \mathbb{E}\left[\lim_{N \rightarrow \infty} \|\theta_{n,N} - \theta_{n,0}\|^2 \right] \leq \liminf_{N \rightarrow \infty} \mathbb{E}[\|\theta_{n,N} - \theta_{n,0}\|^2] \leq \frac{V\eta_0^2}{n-1}.$$

By the Hölder continuity assumption, $d(f_\theta, f_{\theta'}) \leq L\|\theta - \theta'\|^\gamma$. Thus,

$$d(f_{\theta_{n,\infty}}, f_{\theta_{n,0}}) > \frac{\varepsilon}{2} \implies L\|\theta_{n,\infty} - \theta_{n,0}\|^\gamma > \frac{\varepsilon}{2} \implies \|\theta_{n,\infty} - \theta_{n,0}\| > \left(\frac{\varepsilon}{2L} \right)^{1/\gamma}.$$

Applying Markov's inequality to the L^2 bound yields

$$\Pi_n\left(\theta : d(f_\theta, f_{\theta_{n,0}}) > \frac{\varepsilon}{2}\right) \leq \frac{\mathbb{E}[\|\theta_{n,\infty} - \theta_{n,0}\|^2]}{\left(\frac{\varepsilon}{2L}\right)^{2/\gamma}} \leq \frac{V\eta_0^2}{(n-1)\left(\frac{\varepsilon}{2L}\right)^{2/\gamma}}.$$

The triangle inequality implies

$$\{\theta : d(f_\theta, f_*) > \varepsilon\} \subseteq \{\theta : d(f_\theta, f_{\theta_{n,0}}) > \varepsilon/2\} \cup \{\theta : d(f_{\theta_{n,0}}, f_*) > \varepsilon/2\}.$$

and so

$$\begin{aligned} \Pi_n(\theta : d(f_\theta, f_*) > \varepsilon) &\leq \Pi_n(\theta : d(f_\theta, f_{\theta_{n,0}}) > \varepsilon/2) + \Pi_n(\theta : d(f_{\theta_{n,0}}, f_*) > \varepsilon/2) \\ &\leq \frac{V\eta_0^2}{(n-1)\left(\frac{\varepsilon}{2L}\right)^{2/\gamma}} + \mathbf{1}\{d(f_{\theta_{n,0}}, f_*) > \varepsilon/2\} \end{aligned}$$

The above inequality holds for any fixed $X_{1:\infty} \in \mathcal{X}^\infty$. So if $f_{\theta_{n,0}}$ is (d, ε_n) -consistent, it suffices to (i) take F_*^n -expectations on both sides of the last display inequality replacing ε with $\tilde{\varepsilon}_n$, (ii) apply Markov's inequality, and (iii) exploit the assumed properties of $\tilde{\varepsilon}_n$, in order to conclude that $\lim_{n \rightarrow \infty} \Pi_n(d(f_\theta, f_*) > \tilde{\varepsilon}_n) = 0$ in F_*^n -probability.

A.3 Proof of Theorem 3

Before proving the theorem, we write out the conditions required in its statement, which rely on the following definition:

Definition 1. For any two disjoint sets $A, B \subset \mathcal{X}$, the saddle height between them is defined as

$$S(A, B) := \sup_{\gamma \in \Gamma(A, B)} \inf_{t \in [0, 1]} f_*(\gamma(t)),$$

where $\Gamma(A, B)$ is the set of all continuous paths $\gamma : [0, 1] \rightarrow \mathcal{X}$ such that $\gamma(0) \in A$ and $\gamma(1) \in B$.

Based on this definition, the required conditions are:

(a) There exist $C_0, \varepsilon_0 > 0$ such that

$$\forall \varepsilon \in (0, \varepsilon_0), \quad \lambda(\{x \in \mathcal{X} : |f_*(x) - c| \leq \varepsilon\}) \leq C_0 \varepsilon;$$

(b) There exists $\delta_0 \in (0, c)$ such that

$$\max_{i \neq j} S(C_i(f_*), C_j(f_*)) \leq c - \delta_0;$$

(c) There exists $\eta_0 > 0$ such that, for all $\eta \in (0, \eta_0)$:

- For each $j \in \{1, \dots, k_{f_*}\}$, the set $K_j^\eta := \{x \in C_j(f_*) : f_*(x) \geq c + \eta\}$ is non-empty and path-connected.
- $\mathcal{L}_{c-\eta}(f_*)$ has k_{f_*} path-connected components.

To begin the proof, define the event $E_n = \{f : \|f - f_*\|_{\mathcal{L}^\infty} \leq \tilde{\varepsilon}_n\}$. By the posterior contraction assumption (1), $\lim_{n \rightarrow \infty} \Pi_n(E_n^c) = 0$ in F_*^n -probability. Hence, it suffices to show that, for sufficiently large n , $f \in E_n$ implies that $k_f = k_{f_*}$ and $\inf_{\sigma \in S_{k_{f_*}}} \sum_{j=1}^{k_{f_*}} \lambda(C_j(f_*) \Delta C_{\sigma(j)}(f)) \leq k_{f_*} C_0 \tilde{\varepsilon}_n$. To that end, fix n large enough such that $\tilde{\varepsilon}_m < \min(\delta_0, \eta_0)$ for all $m \geq n$, and take $f \in E_n$.

Proof of Equation (2). We first verify that there is a one-to-one correspondence between $\mathcal{C}(f_*)$ and $\mathcal{C}(f)$. Suppose a cluster $C(f) \in \mathcal{C}(f)$ intersects two distinct true clusters $C_i(f_*)$ and $C_j(f_*)$. Since $C(f)$ is path-connected, there exists a path γ contained in it and connecting the two sets. For all x in the range of γ , $f(x) \geq c$, which implies $f_*(x) \geq f(x) - \tilde{\varepsilon}_n \geq c - \tilde{\varepsilon}_n > c - \delta_0$. However, by condition (b), any path between $C_i(f_*)$ and $C_j(f_*)$ must cross a saddle point x_s where $f_*(x_s) \leq c - \delta_0$, yielding a contradiction. Thus, any cluster of f intersects at most one cluster of f_* .

Next, consider the core $K_j^{\tilde{\varepsilon}_n} = \{x \in C_j(f_*) : f_*(x) \geq c + \tilde{\varepsilon}_n\}$. By condition (c), this set is path-connected. For any $x \in K_j^{\tilde{\varepsilon}_n}$, we have $f(x) \geq f_*(x) - \tilde{\varepsilon}_n \geq c$, so $K_j^{\tilde{\varepsilon}_n} \subseteq \mathcal{L}(f)$. Since it is path-connected, $K_j^{\tilde{\varepsilon}_n}$ must be contained in a single component $C_j(f)$ of $\mathcal{L}(f)$.

Combining these findings, for every true cluster $C_j(f_*)$, there exists a unique estimated cluster $C_j(f)$ containing $K_j^{\tilde{\varepsilon}_n}$, which implies $k_f \geq k_{f_*}$. Now consider any $C(f) \in \mathcal{C}_c(f)$. Since $\mathcal{L}(f) \subseteq \{x : f_*(x) \geq c - \tilde{\varepsilon}_n\}$, $C(f)$ is a path-connected subset of the level set $\mathcal{L}_{c-\tilde{\varepsilon}_n}(f_*)$, and is therefore included in one of the clusters of $\mathcal{L}_{c-\tilde{\varepsilon}_n}(f_*)$. By condition (c), there are exactly k_{f_*} such clusters, so that $k_f \leq k_{f_*}$. This completes the proof of the fact that $k_f = k_{f_*}$.

Proof of Equation (3). Define a bijection σ mapping the index j of each true cluster $C_j(f_*)$ to the index of the unique estimated cluster $C_{\sigma(j)}(f)$ containing the core $K_j^{\tilde{\varepsilon}_n}$, as implied by the immediately preceding arguments. Consider the symmetric difference for each pair. If $x \in C_{\sigma(j)}(f) \setminus C_j(f_*)$, then $f(x) \geq c$ and $f_*(x) < c$, implying $c > f_*(x) \geq f(x) - \tilde{\varepsilon}_n \geq c - \tilde{\varepsilon}_n$. If $x \in C_j(f_*) \setminus C_{\sigma(j)}(f)$, then x must lie outside the core $K_j^{\tilde{\varepsilon}_n}$, so $c \leq f_*(x) < c + \tilde{\varepsilon}_n$.

This shows that $C_{\sigma(j)}(f) \Delta C_j(f_*) \subseteq \{x : |f_*(x) - c| \leq \tilde{\epsilon}_n\}$. Using condition (a),

$$\lambda(C_{\sigma(j)}(f) \Delta C_j(f_*)) \leq \lambda(\{x : |f_*(x) - c| \leq \tilde{\epsilon}_n\}) \leq C_0 \tilde{\epsilon}_n.$$

Summing over all clusters, we obtain

$$\sum_{j=1}^{k_{f_*}} \lambda(C_j(f_*) \Delta C_{\sigma(j)}(f)) \leq k_{f_*} C_0 \tilde{\epsilon}_n,$$

which completes the proof.

B EXPERIMENT DETAILS

In this appendix, we provide more details about the numerical experiments presented in the main body of the article.

B.1 NOISY CONCENTRIC CIRCLES

Dataset. We generate $n = 5,000$ two-dimensional observations from two noisy concentric circles using a fixed random seed, with Gaussian noise of standard deviation 0.15 and a radius factor of 0.25. The outer and inner circles contain approximately 4,000 and 1,000 points respectively, reflecting the ratio imposed by the factor parameter. Data are standardized to zero mean and unit variance before fitting.

Density Estimator. We use a Masked Autoregressive Flow (Papamakarios et al., 2017) implemented via the `surjectors` library (Dirmeier, 2024). The architecture consists of 12 alternating MAF layers, each with a MADE conditioner (Germain et al., 2015) comprising two hidden layers of width 128, interleaved with reverse permutation layers. The base distribution is a standard two-dimensional Gaussian. The model is trained by maximum likelihood using AdamW (Loshchilov and Hutter, 2019) with gradient clipping (global norm ≤ 1), weight decay 10^{-4} , and a warmup-cosine decay learning rate schedule peaking at 10^{-3} and decaying to 10^{-6} over 10,000 epochs with batch size 5,000.

Predictive Resampling. We generate $T = 1,000$ independent resamples, each running for $N = 3,000$ score-based update steps with base learning rate $\eta_0 = 0.02$ and effective schedule $\eta_k = \eta_0 / (n + k)$. Gradients are clipped to $[-100, 100]$ and NaN values are replaced with zero for numerical stability. The T resampling chains are executed in parallel on a single GPU.

Clustering Algorithm. The clustering procedure applied to each (trained or resampled) density is described in Algorithm 1. The density threshold τ is set to the 10th percentile of the log-density values of the training data under the initially trained model $f_{\theta_{n,o}}$, and is held fixed across all resamples. The neighborhood radius r is computed adaptively from the training data as 1.2 times the mean 10th nearest-neighbor distance among points above the threshold, and is likewise fixed across resamples. The minimum cluster size is set to $m = 100$.

B.2 MNIST DIGITS

Dataset. We consider a subset of $n = 5,000$ images from the MNIST dataset (LeCun et al., 1998) containing a balanced number of digits 3 and 8. Images are 28×28 grayscale pixels, normalized to $[0, 1]$.

Dimensionality Reduction. Prior to density estimation, images are embedded into a 24-dimensional latent space using a convolutional autoencoder trained with mean squared error reconstruction loss. The encoder consists of three convolutional layers (32, 64, and 128 channels, with stride-2 convolutions and ReLU activations) followed by a linear projection to the latent space; the decoder mirrors this architecture with transposed convolutions. The autoencoder is trained for 25 epochs using Adam (Kingma and Ba, 2015) with learning rate 10^{-3} and batch size 128. Latent codes are standardized to zero mean and unit variance before fitting the flow.

Algorithm 1 Density-Based Clustering via Upper-Level Sets

Require: Data $X = \{x_1, \dots, x_n\}$, log-density values $\{\log f(x_i)\}_{i=1}^n$, threshold τ , radius r , minimum cluster size m

Ensure: Cluster labels ℓ_1, \dots, ℓ_n

- 1: Initialize $\ell_i \leftarrow -1$ for all i
- 2: Identify core points: $\mathcal{D} \leftarrow \{i : \log f(x_i) > \tau\}$
- 3: Build radius neighborhood graph G on $\{x_i : i \in \mathcal{D}\}$ with radius r
- 4: Compute connected components of G ; assign component labels to $\{\ell_i : i \in \mathcal{D}\}$
- 5: Let $\mathcal{K}_{\text{large}}$ be the set of component labels with $\geq m$ members
- 6: Let $\mathcal{K}_{\text{small}}$ be the set of component labels with $< m$ members
- 7: **for all** i with $\ell_i \in \mathcal{K}_{\text{small}}$ **do**
- 8: $\ell_i \leftarrow$ label of the nearest point j with $\ell_j \in \mathcal{K}_{\text{large}}$
- 9: **end for**
- 10: **for all** i with $\ell_i = -1$ **do**
- 11: $\ell_i \leftarrow$ label of the nearest point j with $\ell_j \neq -1$
- 12: **end for**
- 13: Re-index labels to $\{0, 1, \dots, K - 1\}$
- 14: **return** ℓ_1, \dots, ℓ_n

Density Estimator. We fit a MAF (Papamakarios et al., 2017) to the standardized latent codes. The architecture consists of 16 alternating MAF layers, each with a MADE conditioner (Germain et al., 2015) comprising two hidden layers of width 128, interleaved with reverse permutation layers. The base distribution is a standard 24-dimensional Gaussian. The model is trained by maximum likelihood using Adam with learning rate 10^{-4} and batch size 128 for 15 epochs.

Predictive Resampling. We generate $T = 500$ independent resamples, each running for $N = 3,000$ score-based update steps with base learning rate $\eta_0 = 0.002$ and effective schedule $\eta_k = \eta_0/(n + k)$. The T resampling chains are executed in parallel on a single GPU.

Clustering. For each resampled density, clustering is performed using the ToMATo algorithm (Chazal et al., 2013) with a k -nearest-neighbor graph ($k = 20$, brute-force) as the underlying adjacency structure and a fixed merge threshold of 0.5 (visually picked from the ToMATo persistence diagram corresponding to the trained density). Density weights passed to ToMATo are obtained by exponentiating and normalizing the log-density values.

Conformal Credible Set. To assess uncertainty quantification, we apply the conformalized Bayesian inference methodology of Bariletto et al. (2025) using the `cbi_partitions` library. The $T = 500$ posterior clustering samples are split evenly into training (250) and calibration (250) sets. A partition KDE is fitted with the Binder loss metric and bandwidth parameter 0.5. The resulting conformal p -value for the true digit labeling is 0.1952, confirming that the true labeling belongs to a credible set with guaranteed 90% coverage under the MPD.